Progress toward time-resolved molecular imaging: A theoretical study of optimal parameters in static photoelectron holography

S. X.-L. Sun,[1] A. P. Kaduwela,[2,3] A. X. Gray,[1,4,5] and C. S. Fadley[1,4]

[1]*Department of Physics, University of California Davis, Davis, California 95616, USA*

[2]*Air Resources Board, California Environmental Protection Agency, Sacramento, California 95814, USA*

[3]*Department of Land, Air, and Water Resources, University of California Davis, Davis, California 95616, USA*

[4]*Materials Sciences Division, Lawrence Berkeley National Laboratory, Berkeley, California 94720, USA*

[5]*Stanford Institute for Materials and Energy Science, Stanford University and SLAC National Accelerator Laboratory, 2575 Sand Hill Road, Menlo Park, California 94029, USA*

(Received 2 August 2013; revised manuscript received 8 March 2014; published 15 May 2014)

The availability of short-pulse free-electron lasers has led to the idea of using photoelectron holography as a method of directly imaging molecular dissociations or reactions in real time, as, e.g., in a recent theoretical study by Krasniqi *et al.*, [F. Krasniqi, B. Najjari, L. Strüder, D. Rolles, A. Voitkiv, and J. Ullrich, Phys. Rev. A **81**, 033411 (2010)]. In this paper, we extend this earlier work and in particular look at two critical questions concerning the optimum type of data required for such holographic imaging: the choice of photoelectron kinetic energy (e.g., ∼300 eV versus ∼1700 eV as in the prior study), and the use of a single energy or multiple energies. After verifying that our calculations fully duplicate those in this prior paper, we show that using lower energies is preferable to using higher energies for image quality, a conclusion consistent with prior photoelectron holography studies at surfaces, and that multiple lower energies in which the hologram effectively spans a volume in *k*space yields the best quality images that should be useful for such "molecular movies." Although the amount of data required for such multi-energy holography is roughly an order of magnitude higher than that for single energy, the reduction of artifacts and the improved quality of the images suggest this as the optimum ultimate future strategy for such dynamic imaging.

DOI: 10.1103/PhysRevA.89.053415 PACS number(s): 61.05.js, 78.47.jh

I. INTRODUCTION

Photoelectron holography (PH) was originally developed in the surface science community for studying near-surface atomic structure. It was first realized by Szöke [1] that a core-level photoelectron diffraction (PD) pattern could be considered to be a hologram which could be mathematically inverted to produce an image of the atoms around the emitter. Shortly thereafter, Barton [2] extended this idea into a more powerful multi-energy formulation that reduced image distortions and artifacts, including twin images. There have by now been a number of papers discussing the unique merits and limitations of PH compared to other atomic structure methods, including various refinements in the imaging algorithms to further improve structural accuracy [3–11]. As one indicator of activity, the Web of Science presently lists 150 papers involving the topic "photoelectron holography," with interest at the present growing again after an initial burst of activity in the 1990s. Early on, it was also realized that PD effects are present in the angular distributions in core-level photoemission from free molecules [12,13], and that the multiple-scattering theoretical methodologies developed for studies of surface species could be used with small modifications to describe such data [14].

Most recently, with the development of several free-electron laser facilities in the world with unprecedented brightness and pulse widths in the femtosecond regime [15–17], it has been pointed out by Krasniqi *et al.* [18] that PH has the potential for producing real-time "movies" of atomic motion in molecular dissociations and reactions, e.g., as initiated by some sort of pump pulse. These authors have also presented theoretical calculations of single-energy PD patterns and atomic images for a test-case molecule (chlorobenzene) as excited by a hard x ray so as to produce photoelectrons at ∼1700 eV in a feasible experimental geometry and with two different radiation polarizations.

The basic idea of photoelectron holography is illustrated in Fig. 1. The unscattered component of an outgoing core-photoelectron wave is considered the reference wave in a standard holographic description and the scattered components the object waves in the same sense. The measured PD pattern is then the hologram, and is usually normalized by somehow dividing out the intensity profile of the reference wave in the absence of scattering.

The strong forward scattering effects that arise for photoelectrons in the keV range is known to produce image distortions in PH images that can be difficult to correct, and this has led to a proposal to suppress emission in the forward direction by going to a geometry in which the differential photoelectric cross sections are small or zero along the direction pointing toward a given strong scatterer [19]. One can thus speak of a "nodal" plane in the cross section, and for example, this is the plane of directions perpendicular to the light polarization for emission from an *s* subshell.

In this paper, we extend the prior work by Krasniqi *et al.* [18] so as to explore improving the quality of the reconstructed image of the molecular structure in two ways: by exploring the choice of outgoing photoelectron kinetic energy or energies and by asking whether single or multiple photoelectron kinetic energies should be employed to optimize the image quality. It is important to note, however, that going to lower-energy photoelectrons to reduce the degree of forward scattering and enhance the degree of back scattering, and using multiple energies to reduce twin images and reduce image artifacts,

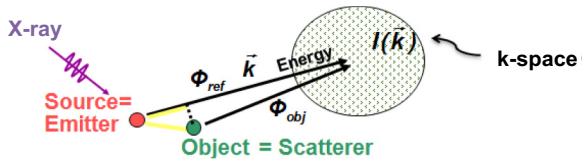

FIG. 1. (Color online) Schematic view of photoelectron holography with sampling of both angle and energy to span a volume in k space: ϕ_{ref} is the reference wave and ϕ_{obj} is the object wave.

have both been found to be more beneficial in several prior PH studies of solids and surfaces [3–8].

II. EXAMPLE SYSTEM AND THEORETICAL METHODOLOGY

In the previous study [18], and also ours, the emitter is the chlorine atom in the chlorobenzene molecule. The excitation is assumed to be from the Cl 1s level core. This level has a binding energy of 2822 eV, such that, with the photon energy of 4522 eV used in the previous study, the kinetic energy will be a relatively high 1700 eV [18]. In addition, because of the dipole selection rule in the photoelectric effect, the emitted photoelectrons will be p waves whose intensity maxima are oriented along the linear polarization vector of the incoming light. Thus, there will be a nodal plane perpendicular to this vector, as shown in Fig. 2, with nonzero photoelectron intensity directly in this plane only being possible via elastic scattering from other atoms in the molecule.

With a fixed geometry between the incoming light and the molecule of interest, there are thus two limiting geometries for photoelectron holography depending on the relative position of the detector. These we refer to as the far-node, with maximum reference-wave intensity from the p-wave character of the photoelectron, and the near-node [18,19], with minimum

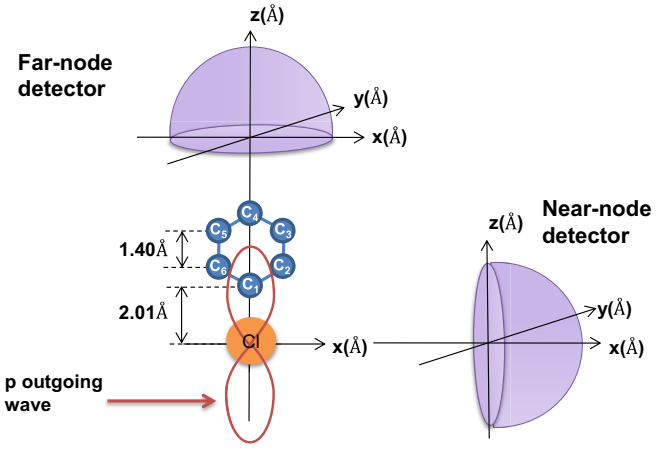

FIG. 2. (Color online) The molecular geometry for the chlorobenzene molecule, C_6H_5Cl, and the two experimental situations simulated. All the carbon atoms are numbered using subscripts 1 to 6. The molecule lies in the x-z plane, and the detector hemisphere is centered along the z axis for the far-node geometry and along the x axis for near-node. The weak-scattering H atoms are neglected.

intensity, as shown in Fig. 2. The far-node PH can also result in strong forward scattering from atoms along the direction to the detector; as noted previously, such forward scattering is known to lead to image distortions and artifacts in PH. The near-node PH was thus proposed as a method to reduce these deleterious forward-scattering effects on holographic images [19].

In the previous study [18] of the chlorobenzene molecule, the theoretical simulations that made use of far-node photoelectron holography considered only three atoms in the cluster, as shown in Fig. 2: the emitter which is the chlorine atom at the origin (0, 0, 0), carbon atom 2, and carbon atom 6. The reason for studying this small fraction of the entire molecular structure is indicated in the original text as being that the two carbon atoms studied are the "active scatterers" [18]. We have thus explored the degree to which other scatterers in the molecule may be important in such PH imaging. For example, a fundamental argument suggests a more realistic treatment: Because carbon atom 1 is closest to a lobe of the p waves coming out of chlorine atom, this carbon atom should scatter photoelectrons more strongly than carbon atoms 2 and 6.

To explore the possibility of PH from this molecule more quantitatively, calculations were first performed to test the degree of agreement of our calculations with those of Krasniqi *et al.*, as, e.g., shown in Fig. 3(a). The actual PD holograms were calculated using an existing online program called Electron Diffraction in Atomic Clusters (EDAC) for core-level photoelectron diffraction simulations [20–22]. This program permits including multiple scattering effects up to arbitrary order, and after carrying out a systematic study at the single-scattering level of using both low and high kinetic energies, we have for a few cases also explored the effects of multiple scattering. Using the same parameters as those in the original study [18] (only two carbon atoms, a single photoelectron energy at 1700 eV, and only first-order scattering, etc.), we calculated a diffraction pattern [Fig. 3(b)] that agrees with the one in the previous study [Fig. 3(a)]. We thus conclude that EDAC provides results that are consistent with this earlier study, confirming the accuracy of both methodologies.

Then, the diffraction pattern of the entire molecule, including the benzene ring of six carbon atoms, was computed, keeping everything else the same [see Fig. 3(c)]. Compared to the diffraction pattern including only two carbon atoms [Figs. 3(a) and 3(b)], the new diffraction pattern clearly changes dramatically. Since the only difference in the inputs for these two simulations is the number of carbon atoms included, one can conclude that it is necessary for a realistic simulation of PH from this molecule to include all six carbon atom scatterers for the purpose of the final holographic reconstructions.

To permit direct comparisons with this prior study, we also note that the window for the diffraction patterns in the previous study [18] is (20 Å^{-1}) × (20 Å^{-1}) in momentum space. From the standard conversion between photoelectron kinetic energy (E) and k vector (k)

$$k(\text{Å}^{-1}) = 0.512\sqrt{E(\text{eV})}, \tag{1}$$

we find that $k = 21.11$ Å^{-1} for energy $E = 1700$ eV, which is the single kinetic energy used in the previous study for the outgoing photoelectrons [18]. In other words, the detection

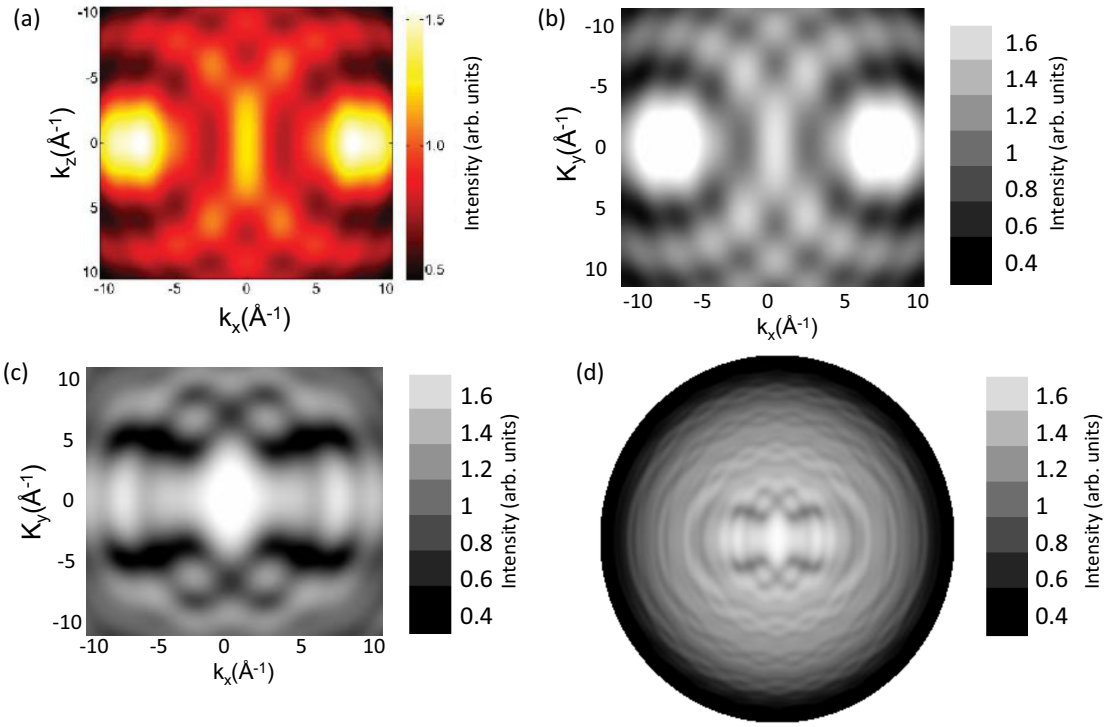

FIG. 3. (Color online) (a) The simulated diffraction pattern using a three-atom cluster (from Ref. [18]). (b) Our simulation for the same cluster, showing excellent agreement. (c) As (b), but for the full seven-atom cluster, and with significant differences. (d) As (c) but over a full hemisphere of detection, corresponding to a radius of 21.11 Å^{-1}. The color bars indicate relative amplitudes of U.

screen was a square cross section in momentum space with a half angle θ as measured from the k_z axis, which corresponds to the $z$axis in Fig. 2 of

$$\theta = \arcsin\left(\frac{10\ \text{Å}^{-1}}{21.11\ \text{Å}^{-1}}\right) \approx 27^{\circ}. \tag{2}$$

We have enlarged this diffraction pattern, again including all six carbon atoms, and have calculated and presented it on an enlarged window which involves $\theta = 90$ degrees away from the Δr axis. We have thus spanned an entire hemisphere with its base in the $k_x - k_y$ plane and a radius of 21.11 Å^{-1}. As shown in Fig. 3(d), this not surprisingly gives a more complete picture for the diffraction pattern and the real-space molecular images presented in this study are all reconstructed from this type of complete hemispheric diffraction pattern.

In the previous study [18], a near-node geometry was also used to simulate a diffraction pattern of the chlorobenzene molecule with all six carbon atoms correctly included [Fig. 4(a)]. This diffraction pattern was calculated exactly in the nodal plane of the outgoing waves with a single energy at 1700 eV. Again for comparison purposes, a simulation was computed using the EDAC online program in this near-node configuration [Fig. 4(b)] and the result agrees very well with the one in the previous paper [Fig. 4(a)].

The scheme for reconstructing the molecular structure in real space from the momentum space hologram is a Fourier-like transform according to Barton's suggestion [2].

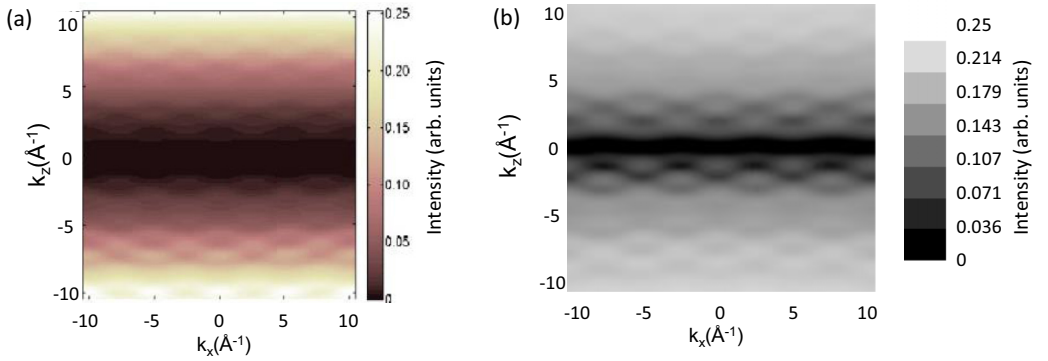

FIG. 4. (Color online) (a) The simulated diffraction pattern in the previous study for six carbon atoms and one chlorine atom in the near-node holography configuration (from Ref. [18]). (b) The diffraction pattern simulated by EDAC using the same parameters as in (a).

We have used the specific implementation of this in the program HOLOINVERT developed by Thevuthasan and Len [23,24], and available for download [25]. Some corrections and updates to this program were made for this study; these are described elsewhere [26].

The inversion of the hologram to produce atomic images is done in two steps. First, the diffraction patterns are normalized with respect to their reference diffraction patterns with no scatterers present. If the measured photoelectron diffraction pattern intensities over some range of wave vectors is $I = (\phi_{obj} + \phi_{ref})^*(\phi_{obj} + \phi_{ref})$ (see Fig. 1), and the photoelectron reference diffraction pattern intensities in the absence of any scatterer is $I_o = \phi^*_{ref}\phi_{ref}$, the normalized diffraction pattern, which is also called the hologram, $H(\hat{k})$ is given by

$$H(\hat{k}) = \frac{I - I_0}{\sqrt{I_0}}. \quad (3)$$

The final step takes a hologram as the input and gives its reconstructed image intensities in real space as the output by computing a Fourier-like integral as introduced by Barton [2]

$$U(\vec{r}) = \left| \iiint H(\vec{k}) e^{[-i\vec{k}\cdot\vec{r} + ikr]} d^3k \right|, \quad (4)$$

where $H(\vec{k})$ is the hologram intensity, the output of the previous normalization program, and $U(\vec{r})$ is the atomic position intensity which represents the holographic estimate of the probability for an atom to be at position $\vec{r}$. This integral is in general over the directions of $\vec{k}$ and the magnitude of Δx if energy is also varied, as in some of the calculations here.

In general, we have considered three aspects of PH beyond those dealt with in the previous study as follows.

(1) As noted above, we have in all of our calculations included all scatterers in the molecule to provide a more realistic picture of the final imaging possible.

(2) We have also considered using both high photoelectron energies at ~1700 keV of the prior study, and lower energies at ~300 eV. It is important to note here that, in order for suitable diffraction to occur, the photoelectron wavelength, which is equal to $\lambda_e(\text{Å}) = \sqrt{\frac{150.4}{E_{kin}(\text{eV})}}$ must be equal to or smaller than the bond lengths in the molecule, the shortest of which is 1.40 Å, corresponding to an energy of 76 eV. Going to too low energies, however, can lead to unfortunate overlap with inelastic and other low-energy secondary electrons. Additional advantages of going to lower energies are that the photoelectric cross section will be higher, for Cl 1*s* increasing by about a factor of 2.4 on going from a kinetic energy of 1700 eV (photon energy of about 4500 eV) to a kinetic energy of 300 eV (photon energy of about 3200 eV) [27] and that the electron atom scattering factor will also be significantly more isotropic in angle, with reduced dominance of forward scattering and enhanced back scattering [27], desirable characteristics for holography. Thus, 300 eV is a reasonable choice for a low energy, with a wavelength of $\lambda_e = 0.70$ Å that is about ½ of the shortest bond length.

(3) Finally, we have explored for both of these energy regimes the use of multi-energy holography as a means of improving images. Specifically, we compare single-energy images at 1700 eV with those reconstructed from ten high energies centered at 1700 eV (1443.64, 1498.78, 1554.95, 1612.15, 1670.45, 1729.88, 1790.18, 1851.52, 1914.06, and 1977.49 eV), as well as single-energy images at 291.34 eV with those reconstructed from ten low-energy levels centered at 291.34 eV (150, 177.42, 207.04, 238.94, 273.11, 309.57, 348.32, 389.35, 432.67, and 478.27 eV). The lowest energy here of 150 eV yields an electron wavelength of 1.00 Å that is smaller than the smallest bond length of 1.40 Å, and is in fact typical of the energies utilized in low-energy electron diffraction to determine surface structures. The energy step for both of the sets of ten high energies and ten low energies here have been chosen such that the steps are on a roughly uniform gird in momentum space of Δk (high) ≈ 0.368 Å^{-1} and Δk (low) ≈ 0.546 Å^{-1} that furthermore matches the grid size in the polar and azimuthal angles of the detector. The angular grid was chosen to be $\Delta\theta = \Delta\varphi = 1°$, so as to yield a reasonably high resolution, as judged by a prior study of optimal sampling in PH [28].

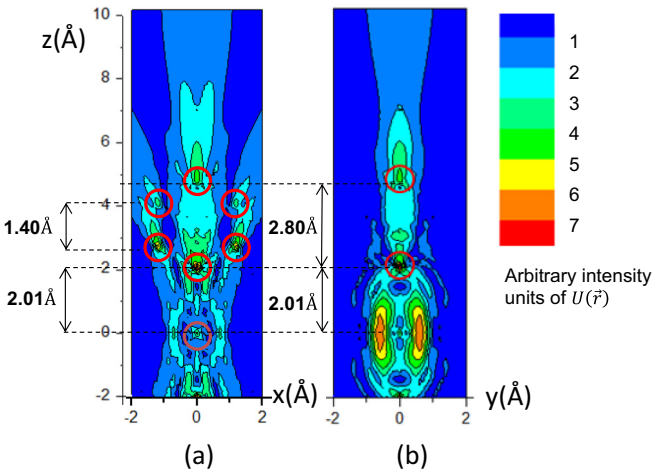

FIG. 5. (Color online) The reconstructed images of the chlorobenzene molecule using a single high kinetic energy of 1700 eV.

III. RESULTS AND DISCUSSIONS

The reconstructed images of the chlorobenzene molecule are plots of atomic position probabilities in three-dimensional real space, and we summarize our results graphically in Figs. 5 to 8. The chlorine atom is at the origin in real space, and we show images with the high symmetry axis of the chlorobenzene molecule along the *z* axis (see Fig. 2). For each set of simulations with different parameters, the reconstructed real space is from −2 to 2 Å in the *x* direction, −2 Å to 2 Å in the *y* direction, and $-2\Delta r$ to 10 Å in the *z* direction. Two perpendicular cross sections are presented below for each set: one is the 4 Å × 12 Å *xz* plane at $y = 0$ and the other one is the 4 Å × 12 Å *yz* plane at $x = 0$. These cross sections show rainbow color-coded contour plots of Δzas defined in Eq. (4). The higher this value is, i.e., the more toward red, the higher the predicted possibility of having an atom at position $\vec{r}$ (*x*, *y*, *z*) in Å. By comparing the peak positions in each contour plot with the ideal positions of the atoms indicated by the red circles in each image, one can semiquantitatively assess the accuracy of the images. Overall, we will assess the degree to which the

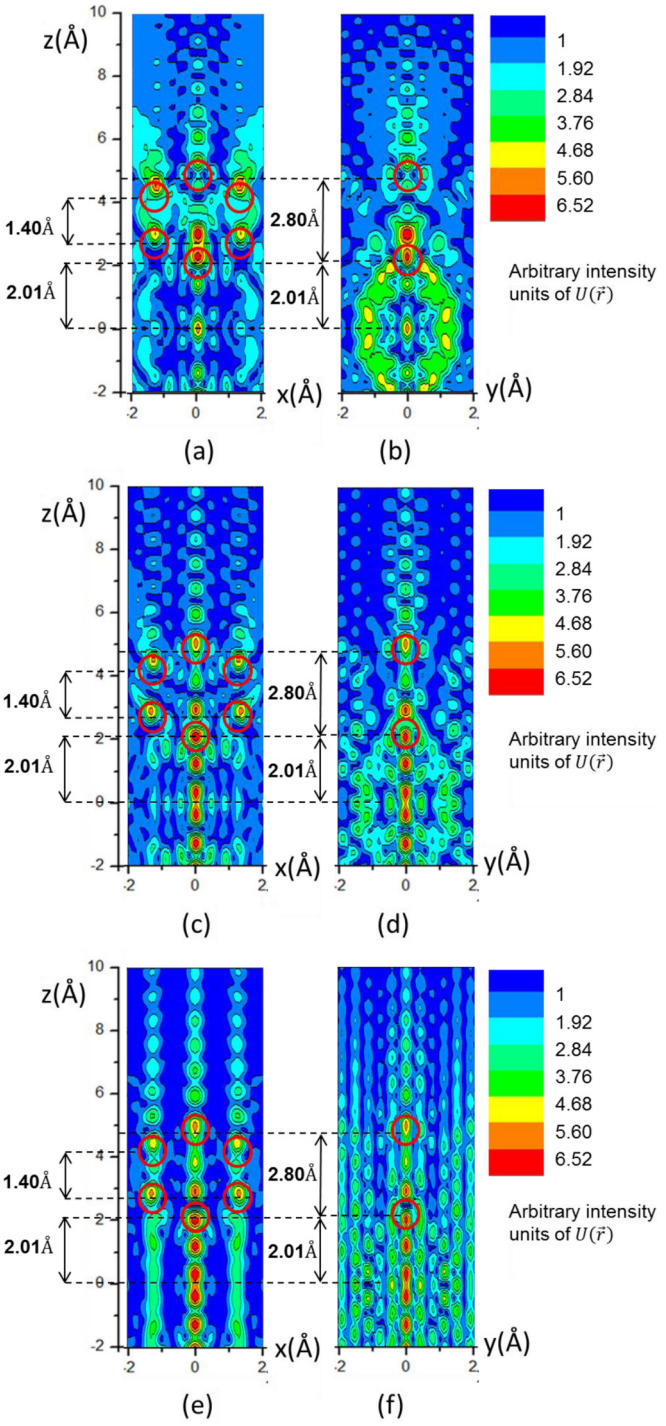

FIG. 6. (Color online) The reconstructed images of the chlorobenzene molecule using a single low kinetic energy of 291.34 eV. (a, b) First-order scattering. (c, d) Second-order scattering (e, f) Third-order scattering.

reconstructed images have pronounced peaks near the ideal positions and a clean background with minimum artifacts.

The cross section in the xz plane at $y = 0$ is expected to show a head-on image of the molecular structure including all six hexagonal carbon atoms, while the cross section in the yz plane at $x = 0$ is expected to only show the carbon atoms 1 and 4 that lie along the z axis. Ideally, the emitter chlorine atom is

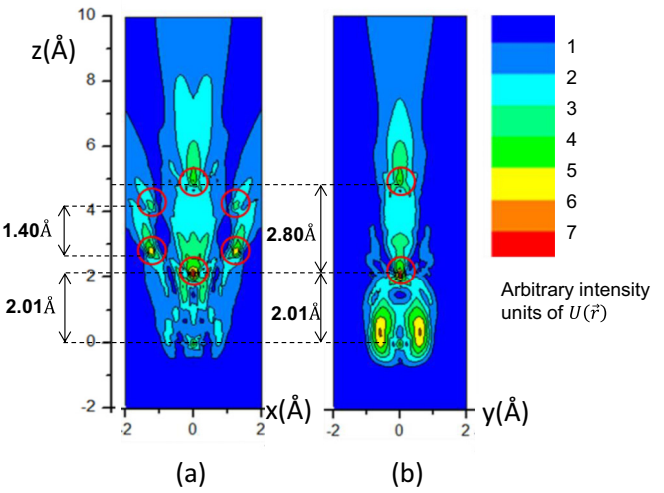

FIG. 7. (Color online) The reconstructed images of the chlorobenzene molecule using multiple high energies.

not expected to be imaged since single scattering is used for these simulations, but it did appear to show up in some images as artifacts, probably due to the I_o normalization procedure used in Eq. (3).

As a further more quantitative global summary of our results Tables I and II show the holographic centroid positions of the atoms for the four cases, $\vec{r}_{Pq}$, with P equaling the atom type and q the atom number, together with the deviations Δx and Δz of these associated image peaks from the ideal position and an estimate of the vector distance deviation from ideal via $\Delta r = \sqrt{(\Delta x)^2 + (\Delta z)^2}$.

A. Images reconstructed with a single high energy

The first set of images (Fig. 5) is reconstructed using a single high photoelectron energy at 1700 eV as an input. In Fig. 5(a), the peak values associated with atoms, which appear to be reddish or greenish in color, fall within the red circles. As expected, the cross section in the xz plane shows the six carbon atoms arranged in a hexagonal shape with bond lengths that agree well with the known structure (Fig. 2). Similarly, the cross section in the yz plane shows the two carbon atoms on the z axis separated by the expected distance. However, the peaks at the atomic positions are not that strong as judged against the overall color scale of both images, largely due to an anomalous double-peaked artifact structure associated with the chlorine emitter. For example, the peaks for the carbon atoms 3 and 5 at about $z = 4$ Å in Fig. 5(a) are very weak.

Another in fact expected artifact, is a mirror image of the molecule below $z = 0$, for which only a portion of carbon atom 1 is shown. This artifact was also present in the previous study of the chlorobenzene molecule [18]. However, this well-known twin-image phenomenon in holography is expected to be suppressed by using multiple energies [2] so it is expected to be suppressed in the simulations that use multiple energies below.

Another interesting observation in these images is that the shapes of the background around the images show streaking at larger distances and seem to mimic the presence of strong

TABLE I. Quantitative assessments of the deviations in atomic positions for single-energy images.

	Single high-energy image					Single low-energy image				
Pq	$U(\vec{r}_{Pq})$	$\vec{r}_{Pq}$ (Å)	Δx (Å)	Δz (Å)	Δr (Å)	$U(\vec{r}_{Pq})$	$\vec{r}_{Pq}$ (Å)	Δx (Å)	Δz (Å)	Δr (Å)
C1	1	(0, 0, 2.1)	0	−0.01	0.01	1 & 0.949	(0, 0, 3) & (0, 0, 2.3)	0	0.99 & 0.29	0.99 & 0.29
C2	0.738	(1.2, 0, 2.8)	−0.01	0.09	0.091	0.77	(1.3,0, 3)	0.09	0.29	0.3
C3	0.46	(1.2, 0, 4.2)	−0.01	0.09	0.091	0.889	(1.3, 0, 4.6)	0.09	0.49	0.498
C4	0.551	(0, 0, 5.1)	0	0.29	0.29	0.685	(0, 0, 5.3)	0	0.49	0.49
C5	0.46	(−1.2, 0, 4.2)	0.01	0.09	0.091	0.889	(−1.3, 0, 4.6)	−0.1	0.49	0.5
C6	0.738	(−1.2,0,2.8)	0.01	0.09	0.091	0.77	(−1.3, 0, 3)	−0.1	0.29	0.31

forward scattering at this high energy, an effect seen before in surface studies with PH [7–9,11].

Table I for this case provides much more quantitative estimates of the position deviations from ideal, and we will discuss these results later for all four sets of calculations.

B. Images reconstructed with a single low energy

Simulations with a single low energy were also conducted to study the effects of using different energy regimes. The results [Figs. 6(a) and 6(b)] have improved from that of a single high-energy images in that the strongest atomic intensity values are of higher relative intensity, although Table I indicates that the lower-intensity atomic positions for the single high energy are in fact somewhat more accurate, with overall upward shifts of 0.3–0.5 Å for low energy, and only 0.01–0.3 Å for high energy. However, since an important final goal of the proposed experiments [18] is to determine the dynamics of the instantaneous molecular structure, i.e., the time dependence of the relative atomic positions, it is the changes in bond lengths that are of most interest. This upward shift is thus not a significant disadvantage of using low energies because the relative bond lengths remain accurate. In addition, the streaking of the images is less pronounced at lower energy, and that fact, combined with the higher relative intensity of the atomic peaks leads us to conclude that low energy would be a more reliable regime in which to work.

This second set of low-single-energy simulations also exposed a few problems that may be further improved using multiple energies. First, as expected for all single-energy images, twin images result. Second, the background artifacts appear to have more oscillatory variations than those of the single high energy.

C. Images reconstructed with ten high energies

Keeping all other parameters the same, this third set of simulations made use of the ten high energies that were specified in Sec. II. Figure 7 shows marked improvements over the single-high-energy results of Fig. 5: the twin images are gone, most peaks are more intense, and Table I indicates an improvement in the vector deviations from the ideal positions, from 0.01–0.3 Å to 0.01–0.09 Å. In general the multi-energy images are cleaner and smoother than the single high-energy images in terms of the background intensities.

Nonetheless, the double-peak structure associated with the emitter, at (0, ± 0.3 Å, 0), although reduced in importance, is still present. We now explore whether this problem can be eliminated by using multiple lower energies.

D. Images reconstructed with ten low energies

The final set of simulations and imaging was carried out with the set of low energies introduced in Sec. II, of course with all the same atomic positions and experimental geometry. Figures 8(a) and 8(b) show that these reconstructed images give the clearest view of the carbon atoms out of all four sets, with no twin images, the double image of the emitter removed, the image streaking reduced, and the artifactual oscillatory features between atoms being reduced, if not eliminated. The contrast between the reconstructed atomic positions and the background is stronger than that in all the previous images. However, the systematic upward shifts of atomic positions by 0.16–0.59 Å associated with multiple low energies remains, and can be compared with the shifts of 0.01–0.09 Å with multiple high energies. Nonetheless, from the point of view of studying atom dynamics, we do not view this as a serious limitation if one considers the other improvements in the low-energy images.

TABLE II. Quantitative assessments of the deviations in atomic positions for multi-energy images.

	Multiple-high-energy image					Multiple-low-energy image				
Pq	$U(\vec{r}_{Pq})$	$\vec{r}_{Pq}$ (Å)	Δx (Å)	Δz (Å)	Δr (Å)	$U(\vec{r}_{Pq})$	$\vec{r}_{Pq}$ (Å)	Δx (Å)	Δz (Å)	Δr (Å)
C1	1	(0, 0, 2.1)	0	−0.01	0.01	1	(0, 0, 2.5)	0	0.49	0.49
C2	0.736	(1.2, 0, 2.8)	−0.01	0.09	0.091	0.656	(1.3, 0, 3)	0.09	0.29	0.3
C3	0.469	(1.2, 0, 4.2)	−0.01	0.09	0.091	0.795	(1.3, 0, 4.5)	0.09	0.39	0.16
C4	0.573	(0, 0, 4.9)	0	0.09	0.09	0.531	(0, 0, 5.4)	0	0. 59	0.59
C5	0.469	(−1.2, 0, 4.2)	0.01	0.09	0.091	0.795	(−1.3, 0, 4.5)	−0.09	0.39	0.16
C6	0.736	(−1.2, 0, 2.8)	0.01	0.09	0.091	0.656	(−1.3, 0, 3)	−0.09	0.29	0.3

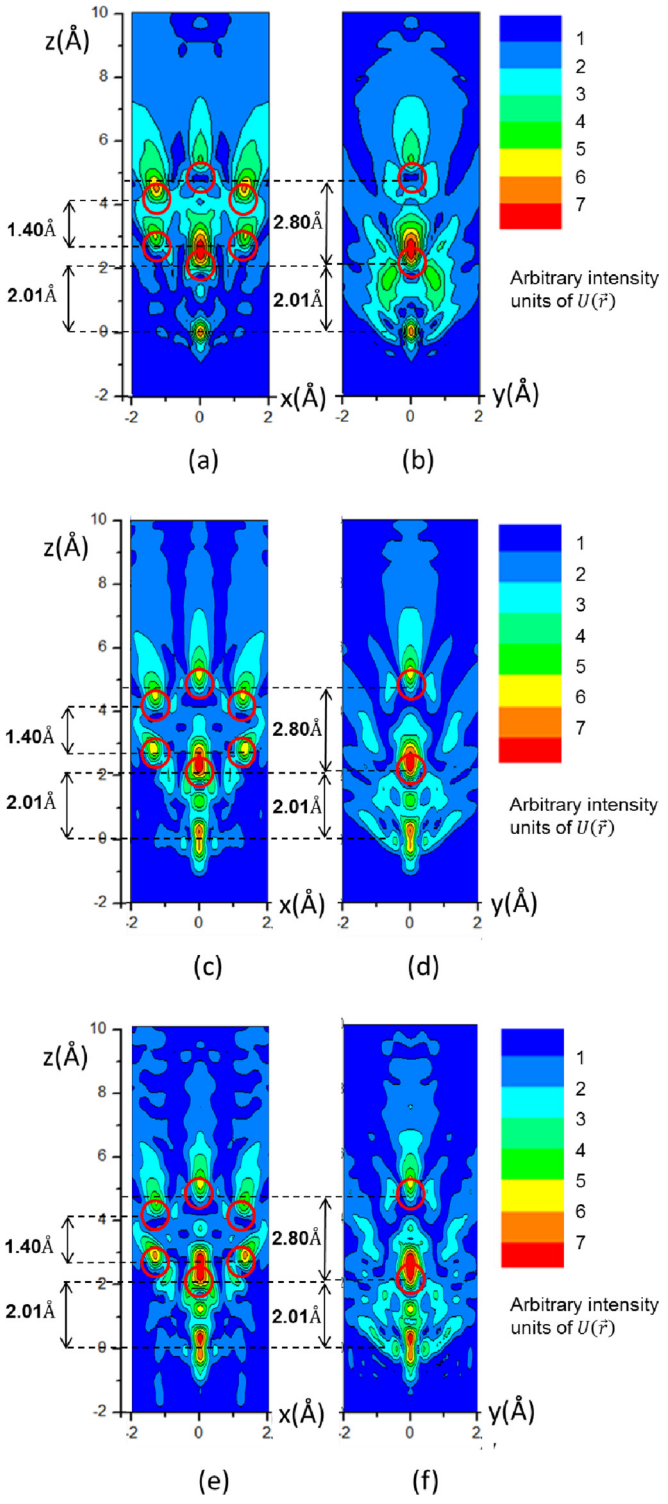

FIG. 8. (Color online) The reconstructed images of the chlorobenzene molecule using multiple low energies. (a, b) First-order scattering. (c, d) Second-order scattering. (e, f) Third-order scattering.

As a general comment, the strongest intensity reconstructed in all four sets of images is carbon atom 1, the atom closest to the origin at $z = 2.01$ Å. This is not surprising, as the outgoing photoelectron wave amplitude decreases as $\frac{1}{r}$ away from the emitter. So this reconfirms that carbon atom 1 is the most important scatterer, as discussed in Sec. II, and must be considered in any holographic modeling.

E. Effects of multiple scattering

Up to this point, our calculations have been in single scattering, but we now consider multiple scattering effects up to third order for the low-energy regime that is really optimal for such holographic imaging. These calculations were carried out just as in our single scattering simulations, assuming a rigid molecular framework with no vibrational attenuation of diffraction due to Debye-Waller-like effects and with no allowance for inelastic attenuation of the photoelectron peak amplitudes, with both of these assumptions expected to be reasonable for a small molecule at room temperature. These simulations should thus represent a conservative estimate of multiple scattering effects. In Figs. 8(c)–8(f), we begin by showing results for our best case of multiple low energies with double and triple scattering, respectively. The atomic positions have actually been somewhat improved in the double-scattering images because the peak intensities are closer to the expected positions and these peaks are also of greater amplitude. The improvements in atomic positions from double to triple scattering are less obvious than those from single to double scattering. These multiple-scattering images for multiple energies also actually exhibit some reduction in the background artifacts, probably due to the cancellation of different phases associated with several interfering multiple scattering paths. The use of multiple energies is thus also found to be robust in imaging even when multiple scattering effects are included. On the other hand, because the final images with multiple energies are not dramatically altered with inclusion of multiple scattering up to third order, we can conclude that single scattering is a decent approximation for simulating holographic imaging for this case.

Turning now to single-energy results with multiple scattering, we show in Figs. 6(c)–6(f) the results for $E = 291.34$ eV with double and triple scattering, respectively. Although the intensities of background artifacts are much reduced at positions other than along the line $x = y = 0$ with the inclusion of multiple scattering, the strong oscillatory artifacts on the line $x = y = 0$ become worse as the scattering order increases, causing considerable confusion as to where the atomic positions should be. Even if we are here making conservative estimates of multiple scattering effects, these results further suggest that single-energy photoelectron holography is a much less robust imaging approach.

IV. CONCLUSION

In summary, based on the four sets of holographic images we have made, three improvements were suggested to the theoretical simulations of far-node photoelectron holography for the example of chlorobenzene, and thus also to experimental methodologies in the future when such exciting dynamics studies become possible.

(1) The nearest-neighbor carbon atom at $z = 2.01$ Å is the most important scatterer in addition to the two carbon

atoms that are indicated as the "active scatterers" in the prior study [18], but all of the scatterers in the molecule must be considered, and can ultimately be imaged.

(2) Using multiple kinetic (or equivalently photon) energies instead of a single energy in dynamic photoelectron holography experiments should yield images with much more accurate atomic positions, including especially the elimination of twin image and other artifacts.

(3) Atomic images become more pronounced and easier to be detected when using low energies in the around 300-eV range instead of higher energies around 1700 eV [18].

(4) Multiple scattering effects up to third order in this low-energy regime do not change multi-energy images appreciably, and using multiple energies very strongly suppresses additional multiple-scattering artifacts that are present in single-energy images.

ACKNOWLEDGMENTS

This work was supported by the Director, Office of Science, Office of Basic Energy Sciences, Materials Sciences and Engineering Division, of the US Department of Energy under Contract No. DE-AC02-05CH11231. Research at Stanford was supported through the Stanford Institute for Materials and Energy Science (SIMES) and the LCLS by the US Department of Energy, Office of Basic Energy Sciences. We also acknowledge helpful comments concerning the software from C. Y. Fong, P.M. Len, and S. Savrasov.

[1] A. Szöke, in *Short Wavelength Coherent Radiation: Generation and Applications*, AIP Conference Proceedings No. 147, edited by D. T. Attwood and J. Boker (AIP, New York, 1986), p. 361.
[2] J. J. Barton, Phys. Rev. Lett. **61**, 1356 (1988).
[3] P. M. Len, J. D. Denlinger, E. Rotenberg, S. D. Kevan, B. P. Tonner, Y. Chen, M. A. Van Hove, and C. S. Fadley, Phys. Rev. B **59**, 5857 (1999).
[4] C. S. Fadley, M. A. Van Hove, A. Kaduwela, S. Omori, L. Zhao, and S. Marchesini, J. Phys. Condens. Matter **13**, 10517 (2001).
[5] T. Matsushita, F. Matsuib, H. Daimonb, and K. Hayashic, J. Electron Spectrosc. Relat. Phenom. **178**, 195 (2010).
[6] C. S. Fadley, J. Electron Spectrosc. Relat. Phenom. **178**, 2 (2010).
[7] B. P. Tonner, Z.-L. Han, G. R. Harp, and D. K. Saldin, Phys. Rev. B **43**, 14423 (1991).
[8] A. Stuck, D. Naumovic, T. Greber, J. Osterwalder, and L. Schlapbach, Surf. Sci. **274**, 441 (1992).
[9] C. S. Fadley, Surf. Sci. Rep. **19**, 231 (1993).
[10] J. Osterwalder, R. Fasel, A. Stuck, P. Aebi, and L. Schlapbach, J. Electron Spectrosc. Relat. Phenom. **68**, 1 (1994).
[11] T. Greber, J. Phys. Condens. Matter **13**, 10561 (2001).
[12] A. Landers, Th. Weber, I. Ali, A. Cassimi, M. Hattass, O. Jagutzki, A. Nauert, T. Osipov, A. Staudte, M. H. Prior, H. Schmidt-Böcking, C. L. Cocke, and R. Dörner, Phys. Rev. Lett. **87**, 013002 (2001).
[13] Th. Weber, O. Jagutzki, M. Hattass, A. Staudte, A. Nauert, L. Schmidt, M. H. Prior, A. L. Landers, A. Brauning-Demian, H. Brauning, C. L. Cocke, T. Osipov, I. Ali, R. Diez-Muino, D. Rolles, F. J. Garcia de Abajo, C. S. Fadley, M. A. Van Hove, A. Cassimi, H. Schmidt-Bocking, and R. Dorner, J. Phys. B, At. Mol. Opt. Phys. **34**, 3669 (2001).
[14] R. Diez-Muino, D. Rolles, F. J. García de Abajo, C. S. Fadley, and M. A. Van Hove, Surf. Rev. Lett. **9**, 1213 (2002).
[15] J. Feldhaus, J. Arthur, and J. B. Hastings, J. Phys. B: At. Mol. Opt. **38**, S799 (2005).
[16] J. Feldhaus, J. Phys. B: At. Mol. Opt. **43**, 194002 (2010).
[17] S. Moeller *et al.*, Nucl. Instrum. Meth. A **635**, Supplement, S6 (2011).
[18] F. Krasniqi, B. Najjari, L. Struder, D. Rolles, A. Voitkiv, and J. Ullrich, Phys. Rev. A **81**, 033411 (2010).
[19] J. Wider, F. Baumberger, M. Sambi, R. Gotter, A. Verdini, F. Bruno, D. Cvetko, A. Morgante, T. Greber, and J. Osterwalder, Phys. Rev. Lett. **86**, 2337 (2001).
[20] F. J. Garcia de Abajo, M. A. Van Hove, and C. S. Fadley, in *Theory and Computation of Synchrotron Radiation Spectroscopy, Frascati, Italy 1999*, edited by M. Benfatto, C. R. Natoli, and E. Pace, AIP Conf. Proc. **514**, 123 (AIP, New York, 2000); Phys. Rev. B **63**, 075404 (2001).
[21] The link to the EDAC program is found at http://nanophotonics.csic.es/index.php?option=com_wrapper&view=wrapper&Itemid=58.
[22] A. P. Kaduwela, D. J. Friedman, and C. S. Fadley, J. Electron Spectrosc. Relat. Phenom. **57**, 223 (1991).
[23] P. M. Len, Ph.D. Thesis, University of California at Davis, 1997.
[24] P. M. Len, S. Thevuthasan, C. S. Fadley, A. P. Kaduwela, and M. A. Van Hove, Phys. Rev. B **50**, 11275 (1994).
[25] The basic files from the Ph.D. thesis of P. M. Len were downloaded from this site: http://www.icts.hkbu.edu.hk/surfstructinfo/SurfStrucInfo_files/holo/holopack.html.
[26] S. X-L. Sun, Senior Honors thesis, University of California at Davis, 2013.
[27] W. Smekal, W. S. M. Werner, and C. J. Powell, Surf. and Interf. Anal. **37**, 1059 (2005); The SESSA program described in this paper was used to estimate the photoelectric and elastic scattering cross sections.
[28] P. M. Len, F. Zhang, S. Thevuthasan, A. P. Kaduwela, C. S. Fadley, and M. A. Van Hove, J. Electron Spectrosc. Relat. Phenom. **85**, 145 (1997).